Journal of Geodynamics 61 (2012) 47–56

Contents lists available at SciVerse ScienceDirect

Journal of Geodynamics

journal homepage: http://www.elsevier.com/locate/jog

Preliminary analysis of the connection between ocean dynamics and the noise of gravity tide observed at the Sopronbánfalva Geodynamical Observatory, Hungary

G. Papp*, E. Szűcs, L. Battha

Geodetic and Geophysical Institute, Research Centre for Astronomy and Earth Sciences, Hungarian Academy of Sciences, Csatkai Endre út 6-8, H-9400 Sopron, Hungary

ARTICLE INFO

Article history:
Received 27 February 2012
Received in revised form 21 June 2012
Accepted 4 July 2012
Available online 25 July 2012

Keywords:
Noise of gravity observations
Sensitivity analysis
Microseisms
Identification of triggering events
Parameterization of events

ABSTRACT

An experimental development of a computer controlled photoelectric ocular system applied for the LaCoste and Romberg G949 gravimeter made the continuous observation of time variation of gravity possible. The system was operated for half a year in the Sopronbánfalva Geodynamical Observatory to test its capabilities. The primary aim of this development was to provide an alternative and self-manageable solution instead of the standard electronic (Capacitive Position Indicator) reading of this type of gravimeter and use it for the monitoring of Earth tide. It, however, turned out that this system is sensitive enough to observe the effect of variable seismic noise (microseisms) due to the changes of ocean weather in the North Atlantic and North Sea regions at microGal level (1 μGal = 10^{-8} m/s^2). Up to now not much attention was paid to its influence on the quality and accuracy of gravity observations because of the large distance (>1000 km) between the observation place (generally the Carpathian–Pannonian basin) and the locations (centres of storm zones of the northern hydrosphere) of triggering events. Based on an elementary harmonic surface deformation model the noise level of gravity observations was compared to the spectral characteristics of seismic time series recorded at the same time in the observatory. Although the sampling rate of gravity records was 120 s the daily variation of gravity noise level showed significant correlation with the variation of spectral amplitude distribution of the analysed high pass filtered (cut-off frequency = 0.005 Hz) seismograms up to 10 Hz. Also available daily maps of ocean weather parameters were used to support both the correlation analysis and the parameterization of the triggering events of microseisms for further statistical investigations. These maps, which were processed by standard image processing algorithms, provide numerical data about geometrical (distance and azimuth of the storm centres relative to the observation point) and physical (mass of swelling water) quantities. The information can be applied for characterizing the state of ocean weather at a given day which may help the prediction of its influence on gravity measurements in the future. Probably it is the first attempt to analyse quantitatively the effect of ocean weather on gravity observations in this specific area of the Carpathian–Pannonian region.

1. Introduction

Nowadays the highest possible accuracy of relative and absolute field observations in gravimetry is better then ±10 μGal (1 Gal = 10^{-2} m/s^2). Therefore the elimination of the time dependent effect of lunisolar (tidal) gravitational forces varying in the range of c.a. ±100 μGal with dominantly diurnal and semi-diurnal periods is one of the most important and routine tasks in the processing of measurements. Global theoretical Earth tide models $\Gamma(t)$ are available (e.g. Wenzel, 1996) for its determination with an accuracy sufficient for general surveying purposes. These models contain the amplitude, frequency and phase parameters of the most important tidal constituents (wave groups) according to the general scheme of spectral synthesis of harmonic signals:

$$\Gamma(\varphi, t) = \sum_{i=1}^{N} a_i(1 + \delta_i) \cos\left(\frac{2\pi}{T_i} t + \Delta\Phi_i\right) \quad (1)$$

where N is the number of harmonic constituents, φ is the latitude of the observation point, $a_i = a_i(\varphi)$ is the amplitude and T_i is the time period of the of the ith constituent, respectively. Parameters a and T (Table 1) can be determined with very high precision from

* Corresponding author. Tel.: +36 99 508364.
E-mail address: papp.gabor@csfk.mta.hu (G. Papp).

0264-3707/$ – see front matter © 2012 Elsevier Ltd. All rights reserved.
http://dx.doi.org/10.1016/j.jog.2012.07.004

Table 1
The most dominant spectral components of gravity tide computed for φ = 47.6° (after Baker, 1984).

Spectral component	Description	T_i period [hours or day]	a_i amplitude [µGal]
Semi-diurnal			
M_2	Main lunar component	12.42	34.1
S_2	Main solar component	12.00	15.8
N_2	Lunar elliptic component elliptikus tag	12.66	6.5
K_2	Luni-solar declination comp.	11.97	4.3
Diurnal			
O_1	Main lunar component	25.82	30.9
K_1	Luni-solar declination component	23.93	43.5
P_1	Main solar component	24.07	14.4
Long periodic			
M_f	Lunar fortnightly component	13.66 d	4.1
M_m	Lunar monthly component	27.55 d	2.1
S_{sa}	Solar semi-annual component	182.62 d	1.9

both direct and indirect effects of interplanetary forces (the mass attraction of the Sun, the Moon, Jupiter,. . .). The indirect effect (i.e. the gravitational effect of the elastic response/deformation of the Earth's body to the interplanetary forces) determines the perturbations δ_i and $\Delta\Phi_i$.

The experimental testing and evaluation of the models of $\Gamma(t)$ at a given geographical location (for some early investigations in the Carpathian–Pannonian region see, for example, the studies of Varga et al., 1977, 1985; Meurers, 1987) can be done by at least half a year gravity tide observations ($\hat{\Gamma}(\varphi, t)$) providing at least ±1 µGal accuracy. Although it is enough for the usual practical requirements of gravimetry and the accuracy is basically available from a technical point of view, the general environmental conditions of the observations may degrade the quality of observations to a great extent. As it will be demonstrated, the noise

$$\nu(\varphi, t) = \hat{\Gamma}(\varphi, t) - \Gamma(\varphi, t) \tag{2}$$

which is defined as a momentary deviation between the measured and predicted/theoretical gravity tide applying the condition $M\{\nu(\varphi, t)\}_{t_1}^{t_2} \cong 0$, where $M\{\}$ stands for the average of noise in the time period between t_1 and t_2, may have a value significantly higher than the amplitude a_i of some tidal constituents (Table 1). The characteristics of the noise, its time variation and their relation to ocean weather processes are discussed in the following sections, based on the observations at Sopronbánfalva Geodynamical Observatory, Sopron, Hungary.

2. General environmental conditions of observations

Gravimetric measurements are influenced strongly by seismic and the so-called microseismic motion of the media forming the body of the Earth (Longuet-Higgins, 1950). Both motions are related to those elastic waves that are excited by either natural or anthropogenic dynamical processes (e.g. earthquakes, weather phenomena on the lands and oceans, and traffic) and propagate in the Earth's interior and on its surface up to a distance basically determined by the energy of the excitation (Gerstoft et al., 2008). The waves deforming the body of the Earth cause both geometrical (surface deformation) and physical (mass redistribution) changes of the media they go through and generate direct and indirect gravitational effects, respectively. Restricting the discussion to vertical displacements (usually these have the most dominant effect on gravity measurements) it means basically that the measuring point changes its height above a reference level through time. So the distance of the point from the centre of mass of the Earth is also changed. If the co-linearity between the plumbline, along which the orthometric height H is defined and the radius vector r going through and pointing to the observation point is assumed then it can be modelled by a simple spherical approximation (e.g. Torge, 2001):

$$\frac{\partial g}{\partial H} \cong \frac{\partial g}{\partial r} = -\frac{2GM_E}{r^3} \tag{3}$$

where $g = GM_E/r^2$ gives the spherically symmetric gravitational field of the mass M_E representing the total mass of the Earth. G is the universal gravitational constant. This approximation is valid on and outside of the surface of the Earth, where the field is harmonic according to the Laplace equation:

$$\Delta V = \frac{\partial^2 V}{\partial x^2} + \frac{\partial^2 V}{\partial y^2} + \frac{\partial^2 V}{\partial z^2} = 0 \tag{4}$$

where V is the gravitational potential.

Although (3) is a very simple model of the Earth's gravity field, it provides sufficient accuracy for the estimation of the direct gravitational effect of the vertical displacement ΔH of the observation point:

$$\Delta g = \frac{\partial g}{\partial H}\Delta H \cong -0.3086 \quad [\text{mGal/m}] \cdot \Delta H \quad [\text{m}] \tag{5}$$

applying the recent value of the geocentric gravitational constant $GM_E = 398600.5 \times 10^9\ \text{m}^3\,\text{s}^{-2}$ and the mean radius of the Earth $r = R = 6371$ km (Torge, 2001). (5) gives approximately −3 µGal gravity change for +1 cm vertical displacement (uprising) of the Earth's surface, but this magnitude of deformation is rarely caused by teleseismic waves generated by distant ($D \geq 1000$ km) events which are the objectives of this recent investigation. It rather characterizes the size of tidal deformations (about from −30 cm to + 50 cm) having low frequency excitation (Melchior, 1966). The non-gravitational ground accelerations generated by them are however, very small. To prove it let us assume that the movement of a point fixed to the Earth's surface is harmonic. Then its vertical motion can be described by a simple, single wave model:

$$H(t) = H_0 + A \sin\left(\frac{2\pi}{T}t\right) \tag{6}$$

where $H_0 = H(t = 0)$ is the reference height of the point, A is the amplitude and T is the cycle time of the motion, respectively. The non-gravitational acceleration of the point can be described by the second time derivative of (6):

$$a(A, T, t) = \frac{d^2H}{dt^2} = -A\frac{4\pi^2}{T^2}\sin\left(\frac{2\pi}{T}t\right) \tag{7}$$

For an approximately diurnal tidal deformation (T = 86,400 s, A = 30 cm) the acceleration resulted by (7) can be seen in Fig. 1. It clearly shows that the peak acceleration hardly reach a = 0.15 µGal which is just a fraction of the change of tidal accelerations (the result of direct and indirect gravitational effects) listed in Table 1.

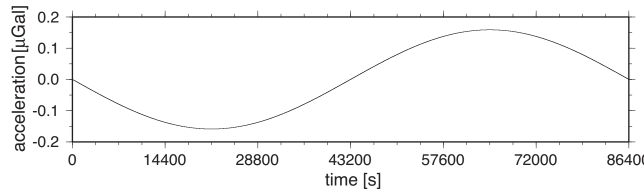

Fig. 1. Synthetic ground acceleration caused by a single wave (harmonic) deformation model of the Earth surface (T = 86,400 s, A = 30 cm in Eq. (7)).

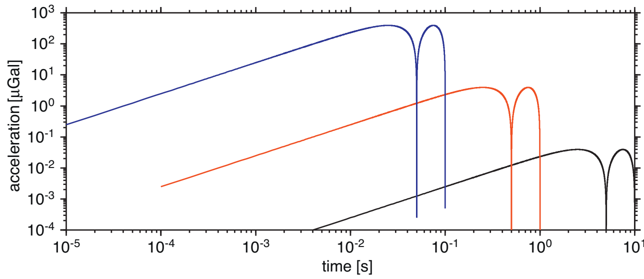

Fig. 2. Synthetic single wave ground accelerations caused by seismic activity. Blue curve: $A = 1$ nm, $T = 0.1$ s, red curve: $A = 1$ nm, $T = 1$ s, black curve: $A = 1$ nm, $T = 10$ s. For every curve a full period is plotted. Note the logarithmic scale for both time and the acceleration values.

Since $a(A,T,t)$ in (7) linearly depends on A but at the same time it is a quadratic function of the frequency, small displacements in the range of a few nm may give high acceleration for periodical motions caused by seismic activity having frequencies in the range between 0.1 Hz and 10 Hz (Fig. 2).

Fig. 2 explains why gravimetric measurements are so influenced by (micro)seismic activity induced by either natural or anthropo-technogenic sources. 1 nm displacement is comparable to atomic dimensions, so it is very difficult to find places on the Earth where the seismic "background" noise (i.e. the periodical movement of the observation point) is negligible from the viewpoint of gravimetry.

It is assumed that other local, for example, underground hydrological effects do not influence the hourly/daily noise level, because these are rather observable in the time dependent characteristics of long term ($T \geq 24$ h) instrumental drift.

3. The noise level of gravimetric observations between 08.06.2010 and 04.01.2011 in Sopronbánfalva Geodynamical Observatory

The LaCoste-Romberg (LCR) G949 gravity meter equipped by a PC controlled Charge Coupled Device (CCD) ocular (Papp et al., 2009) was used to record gravity variations continuously in Sopronbánfalva Geodynamical Observatory operated by the Geodetic and Geophysical Research Institute of the Hungarian Academy of Sciences. Although this system is not conformable with the recent standard high tech Earth tide monitoring instruments (e.g. superconducting gravity meters) the sensitivity of the meter itself (<1 μGal, see e.g. Pálinkáš, 2006) is definitely sufficient for background noise observations as is demonstrated in the following sections. A similar solution was used to improve the accuracy of optical readout of an LCR G meter by Woo et al. (2007).

There are also a Streckeisen STS-2 broadband seismometer and a 20 m long extensometer (Mentes and Eper-Pápai, 2006) installed in the tunnel system of the observatory driven in an outcrop of bedrock formed by gneiss. The site is rated as one of the most "silent" seismological stations in the Carpathian–Pannonian region regarding the observation noise of technogene origin (Tóth et al., 2010) and it is also supposed that the groundwater level variation in the solid bedrock has no significant influence on any kind of geodynamical observables. Some further details about the station SOP, the noise spectrum and the on-line seismogram can be obtained from the Internet (http://www.seismology.hu/index.php/en/observatory/stations).

The sampling rate of gravity observation was only 120 s, because the primary aim was to test the system for Earth tide monitoring and to check the long term behaviour of the gravity meter itself especially the drift. Since the effect of microseisms is observed typically between $1\,\text{s} \leq T \leq 20\,\text{s}$, the direct spectral comparison of gravity time series and the time series of seismic ground accelerations is impossible. The synthetic ground deformation model (Section 2) constrained with the amplitude spectra of observed ground deformation time series, however, can be indirectly used to justify statistically that the increased level of ground accelerations are above the sensitivity limit of the LCR G meter.

5143 h of observations (154,290 samples) were used to determine the hourly noise level of measurements. First the measured values were reduced by a theoretical tidal effect computed from a tidal parameter set (amplitude and phase parameters) derived from long-term observations of the Austrian superconducting gravity meter (Meurers et al., 2007) installed now in Conrad Observatory. ETERNA 3.4 modelling software (Wenzel, 1996) was used to produce $\Gamma(\varphi,t_i)$ function. Because of the lack of proper calibration of the instrument in the range of tidal accelerations (c.a. ±(100–150) μGal) a residual tidal signal of c.a. ±(5–15) μGal characterizes the residual curve. To eliminate the effect of scale difference between observed and theoretical tides the daily scale factor m_d of the instrument was determined and applied to obtain hourly residuals with negligible mean value according to (2):

$$\Delta\hat{g}^{res}_{d,k,l} = (\hat{g}^{obs}_{d,k,l} - \bar{g}^{obs}_{d,k}) - m_d(\Gamma_{d,k,l} - \bar{\Gamma}_{d,k}) \tag{8}$$

$$\bar{g}^{obs}_{d,k} = \frac{1}{L}\sum_{l=1}^{L}\hat{g}^{obs}_{d,k,l} \tag{9}$$

where $\hat{g}$ is the gravimeter reading automatically determined by the computer driven CCD ocular, $\bar{\Gamma}$ is the hourly average of Γ tidal accelerations, $d = 1, 2, \ldots, 214$ is the number of the observation day, $k = 1, 2, \ldots, 24$ is the number of hours on that specific day, $l = 1, 2, \ldots, L = 30$ is the row number of the observations with 2 min sampling rate in the corresponding hour and $\bar{g}$ is the hourly mean value of observations. The influence of the mostly linear instrumental drift which was typically 1 μGal/h in the investigated time period was neglected in the estimation of hourly noise level defined as the RMS dispersion of hourly residuals:

$$\sigma^{obs}_{d,k} = \pm\sqrt{\frac{\sum_{l=1}^{L}(\Delta\hat{g}^{res}_{d,k,l})^2}{L-1}} \tag{10}$$

From Fig. 3 one can see immediately the difference between silent and noisy days. Obviously, the largest dispersions (≫±5 μGal) are mostly caused by distant seismic events, which can be characterized by strong surface waves. But from time to time there is a significant increase in the background noise level (microseisms) when no remarkable teleseismic activity was recorded with the seismometer, otherwise. Furthermore one can clearly distinguish between summer and the autumn-winter period, where generally low and high noise levels are indicated, respectively. Whereas the silent day observations can be characterized by $\sigma = \pm 1$ μGal dispersion the noise level can be a multiple of that (±(4–5) μGal) on noisy days. This seasonal phenomenon is certainly not connected to any kind of anthropogenic activities (e.g. city traffic). Although its reason is known as the seasonal variation of the weather conditions in the North Atlantic and North Sea region (Longuet-Higgins, 1950; Gerstoft et al., 2008; Hillers et al., 2012) it was supposed that gravimetric measurements are hardly influenced by it in the central part of the European continent.

4. Sensitivity analysis of gravity observations by spectral analysis of seismograms

Based on (7) the maximum ground acceleration for any displacement A and cycle time T can be estimated. This way function:

$$a_{\max}(A,T) = a\left(A, T, t = \frac{T}{4}\right) = abs\left(-A\frac{4\pi^2}{T^2}\right) \tag{11}$$

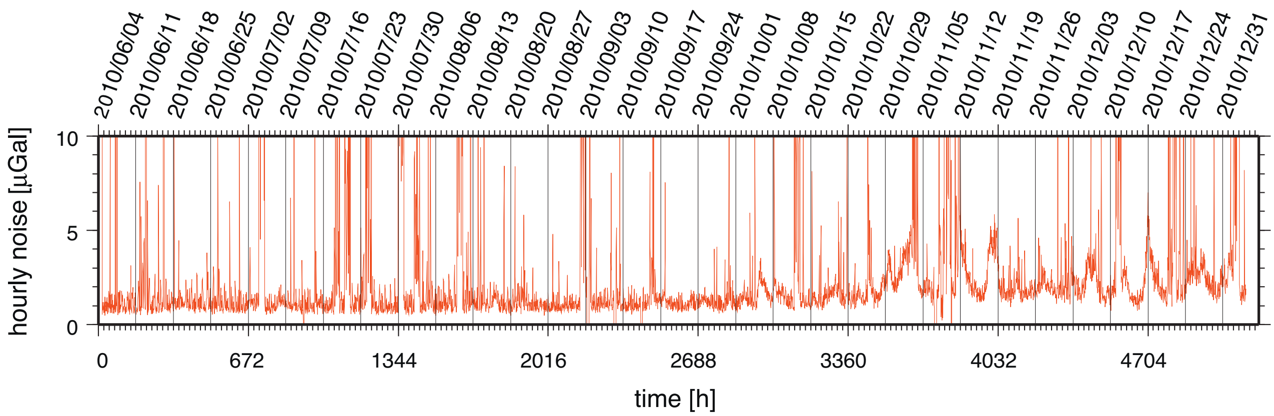

Fig. 3. Hourly noise of gravity tide observations with LCR G949 instrument in Sopronbánfalva Geodynamical Observatory, Hungary.

over two parameters A and T can be defined from (7) and compared to seismological data which are basically recorded as time series of ground velocities $v(t_n)$. Integrating the velocities by a simple numerical approximation:

$$d(t_n) = \sum_n v(t_n)\,\Delta t \tag{12}$$

where Δt is the sampling interval of the continuous $v(t)$ function, one can determine a discrete approximation of the continuous displacement function $d(t)$. The Fourier transform of $d(t)$:

$$D(f) = \int_{-\infty}^{\infty} d(t)e^{2\pi i f t}\,dt \tag{13}$$

defines the Fourier spectrum $D(f)$ of the signal $d(t)$ which is basically the spectral distribution of harmonic components having frequency f. Its integral over the frequency domain (inverse Fourier transform) defines the displacement function (Meskó, 1984):

$$d(t) = \int_{-\infty}^{\infty} D(f)e^{-2\pi i f t}\,df \tag{14}$$

Since digital seismograms are discretely sampled time series and have finite length the tools of discrete Fourier analysis/transform have to be used to determine the discrete spectrum $D(f_m)$:

$$D(f_m) = \sum_{n=0}^{N-1} d(t_n)e^{2\pi i n m/N} \tag{15}$$

where n is the index of samples in the time series of $d(t)$ and m is the index of discrete frequencies:

$$f_m = \frac{m}{N\Delta t}, \qquad m = -\frac{N}{2}, \ldots, \frac{N}{2} \tag{16}$$

Computing the one-sided amplitude spectrum (Press et al., 1986) of the displacement function (12) and using the following identity:

$$D(f_m) = A(f_m) = A\left(\frac{1}{T_m}\right) \tag{17}$$

one can define (17) as a domain for a_{max} given by (11). If both a_{max} and $A(f_m)$ are represented in the same parameter space determined by T and A a simple visual estimation of a_{max} is also possible.

To test the applicability of the scheme given above 3 days were selected from the time period of investigation based on Fig. 3. Both the seismological and gravimetric data recorded on the 8th of June, 5th of October and 2nd of November from the year of 2010 are supposed to represent the statistical/spectral characteristics of observation days having low, moderate- and high background noise level but without sensible (tele)seismic event (Fig. 4).

Only the Z components of the digital seismograms $v(t_n)$ were used for spectral estimation but prior to it the components having long cycle time ($T > 200$ s) were removed by a 2nd order Butterworth high-pass filter. The filtered data were converted to $d(t)$ by (12) afterwards. The amplitude spectra of the pre-processed ground displacement time series of these days and a_{max} function (Eq. (11)) are displayed together in Fig. 5 where the spectra represent the domain for the evaluation of a_{max}.

It is clearly indicated that during a "silent day" (grey line) the main source of microseismic tremor of the observation point is in the frequency range above 2.5 Hz ($T \le 4 \times 10^{-1}$ s), where the amplitude of the spectral components may produce ± 1 µGal maximum ground acceleration (0 contour line for $\log_{10}(a_{max})$). A "moderately noisy" day (blue line) shows increased amplitudes between 0.05 Hz and 1 Hz ($1\text{ s} \le T \le 20$ s) the source of which is generally identified as the ocean weather in the North Atlantic and North Sea region for seismological stations located on the European continent. The peak amplitude for this spectrum is about 30 nm, but just a few spectral components in a narrow cycle time band around $T = 8$ s can cause ground acceleration higher than ± 1 µGal (see the area between contour lines of 0 and 1 values). The daily average noise level is about ± 2 µGal on this day (Fig. 4). The red curve representing the amplitude spectrum of a signal with high noise level indicates a well-defined, compact band ($4\text{ s} \le T \le 7$ s) of increased amplitudes (related to the blue and grey curves) where most of the components can generate about ± 2 µGal maximum ground accelerations. Concerning the width of this band it is at least 3 times larger than what

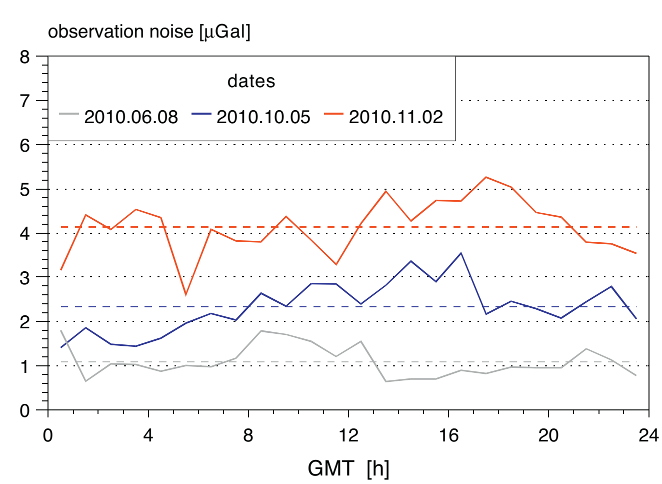

Fig. 4. Hourly noise plots for gravity tide observations at Sopronbánfalva Geodynamical Observatory. The dashed lines represent the daily average noise levels.

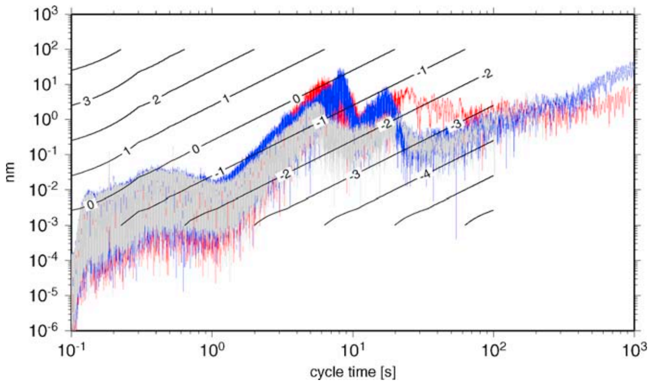

Fig. 5. A combined plot of amplitude Fourier spectra of Z displacement functions and the contour line map of maximum single wave ground acceleration ($\log_{10}(a_{\max})$) as function of cycle time and maximum displacement. The spectra represent the domains for the evaluation of $a_{\max}$. Red – 2010.11.02, blue – 2010.10.05, grey – 2010.06.08. Note the logarithmic scale both for coordinate axes and for the contour lines.

can be seen on the blue curve. Consequently the sum of the components having close cycle time may result in several μGal peak acceleration of the ground which is also indicated in Fig. 4, where the daily average noise level is above of ±4 μGal on this specific day.

One should note that the noise seems to be quite stationary in the interval between 1 s and the Nyquist period (0.1 s) and independent from the pregnant variations in the frequency band below 1 Hz. Therefore the increased gravity noise level is certainly connected to processes generating low frequency (<1 Hz) deformations of the ground below the observing instrument.

5. Identification of the triggering events of increased observation noise

It is commonly supposed that the main source of microseisms observed on the European continent is the interaction between processes of the atmosphere and hydrosphere in the North Atlantic and North Sea regions. This interaction is the subject of ocean weather research. One of its main tasks is to monitor the dynamics of the processes in real time, so nowadays maps

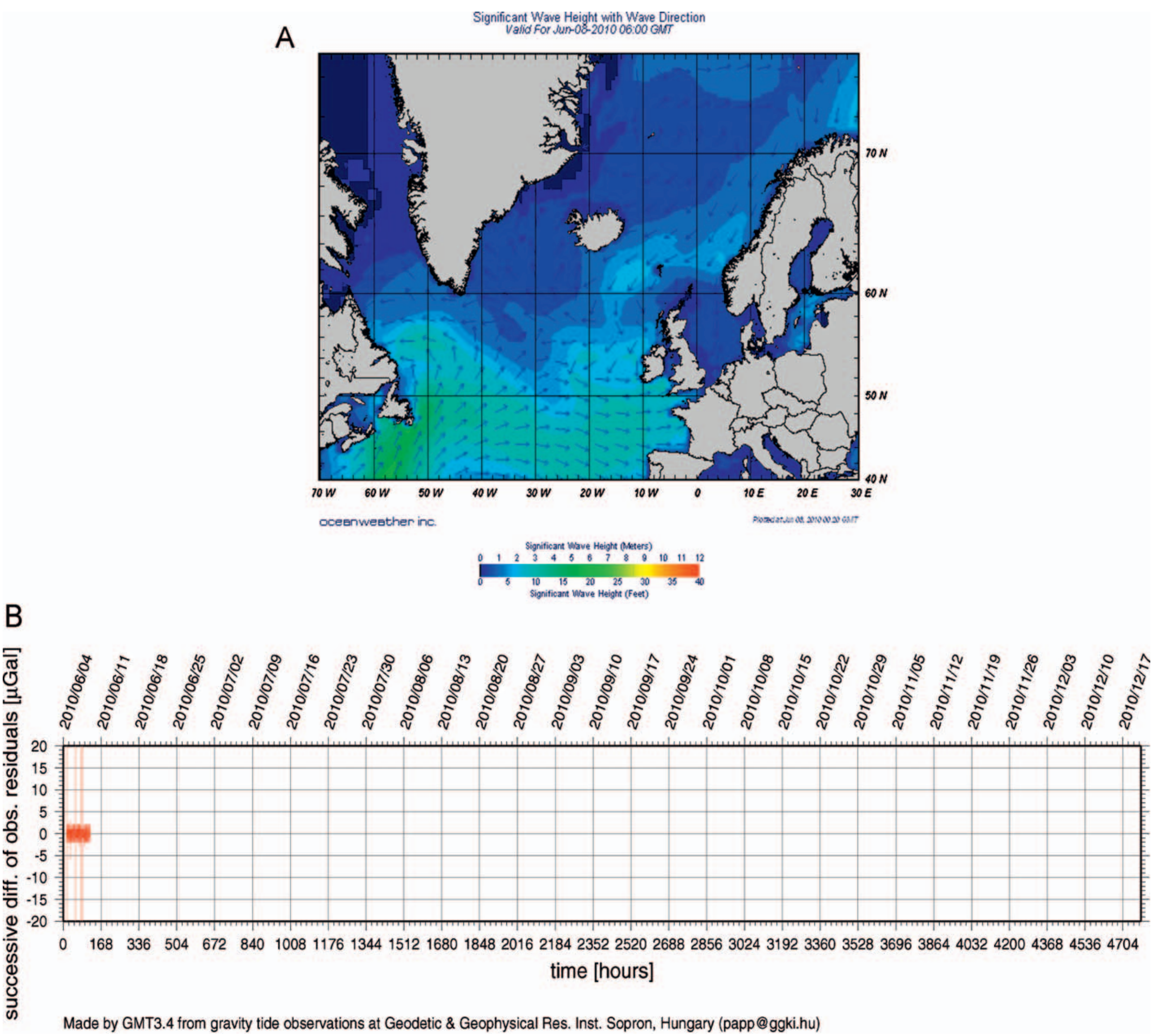

Fig. 6. Ocean weather map (top) and the noise of gravity tide observations in Sopronbánfalva Geodynamical Observatory (bottom) on 08.06.2010. The arrows show the wave directions.

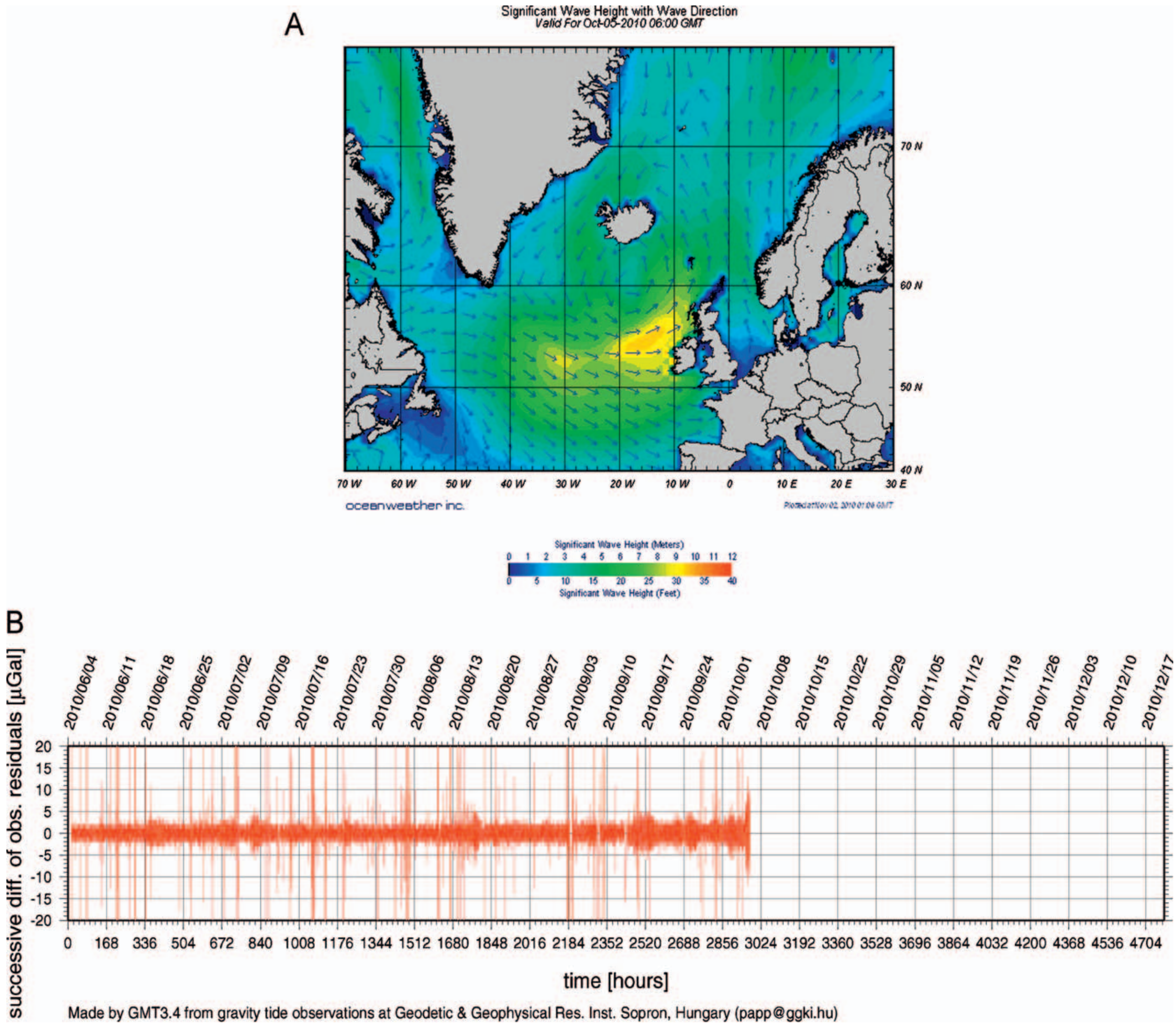

Fig. 7. Ocean weather map (top) and the noise of gravity tide observations in Sopronbánfalva Geodynamical Observatory (bottom) on 05.10.2010. The arrows show the wave directions.

of different ocean weather parameters updated daily or even more frequently are accessible from the World Wide Web (e.g. www.oceanweather.com). Therefore the noise level variation in both gravimetric and seismological observations can be checked against the momentary state of the hydrosphere described by different marine data (e.g. so-called significant wave height H_{sw}, wave direction).

In order to demonstrate the connection between observation noise level and the weather conditions on the oceans, the time series of the successive differences of observation residuals are compared to the significant wave height maps of the days included in the time series. The maps and viewgraphs paired for the specific days investigated can be seen in Figs. 6–8. Because of the large number of these daily snapshots the easiest way of the process visualization is a moving picture made of them (the reader is referred to http://www.ggki.hu/eng/news).

Besides the visual correlation clearly demonstrating the strong influence of heavy swell in the North Atlantic region on the noise of the recorded gravity tide an effort was made to quantify at least statistically this relationship. The driving mechanism of microseisms, however, is not as simple as implied by this observational approach. Whereas the contribution of the coastal waves (primary microseisms) is rather straightforward, the mechanism of the secondary microseisms generated by the so-called standing waves is more complex and non-linear (Longuet-Higgins, 1950; Kedar, 2011). It can be investigated only by so-called wave-wave interaction models (see e.g. Kedar et al., 2008; Hillers et al., 2012) based on which the interaction intensity (Ψ) maps can be derived/hindcasted. These clearly indicate that, although the triggering events are wave generating storms on the oceans, in general the storm wave centres are geographically different from the source locations of secondary microseisms where $\Psi = \Psi_{max}$. Obviously, in this context this investigation can be regarded as a preliminary, phenomenological approach because only few parameters were determined from marine data web-distributed by Oceanweather Inc. (www.oceanweather.com) to characterize the interaction between the triggering events and the noise at observation place. The significant wave height H_{sw} was the basic quantity of this parameterization. The areal distribution of its intensity can determine several parameters: the location of maximum wave height, the extension of swelling/stormy area, the mass/volume and barycentre of swelling water (referred as storm centre later on), spherical distance and azimuth between the centre and the observation place, etc.

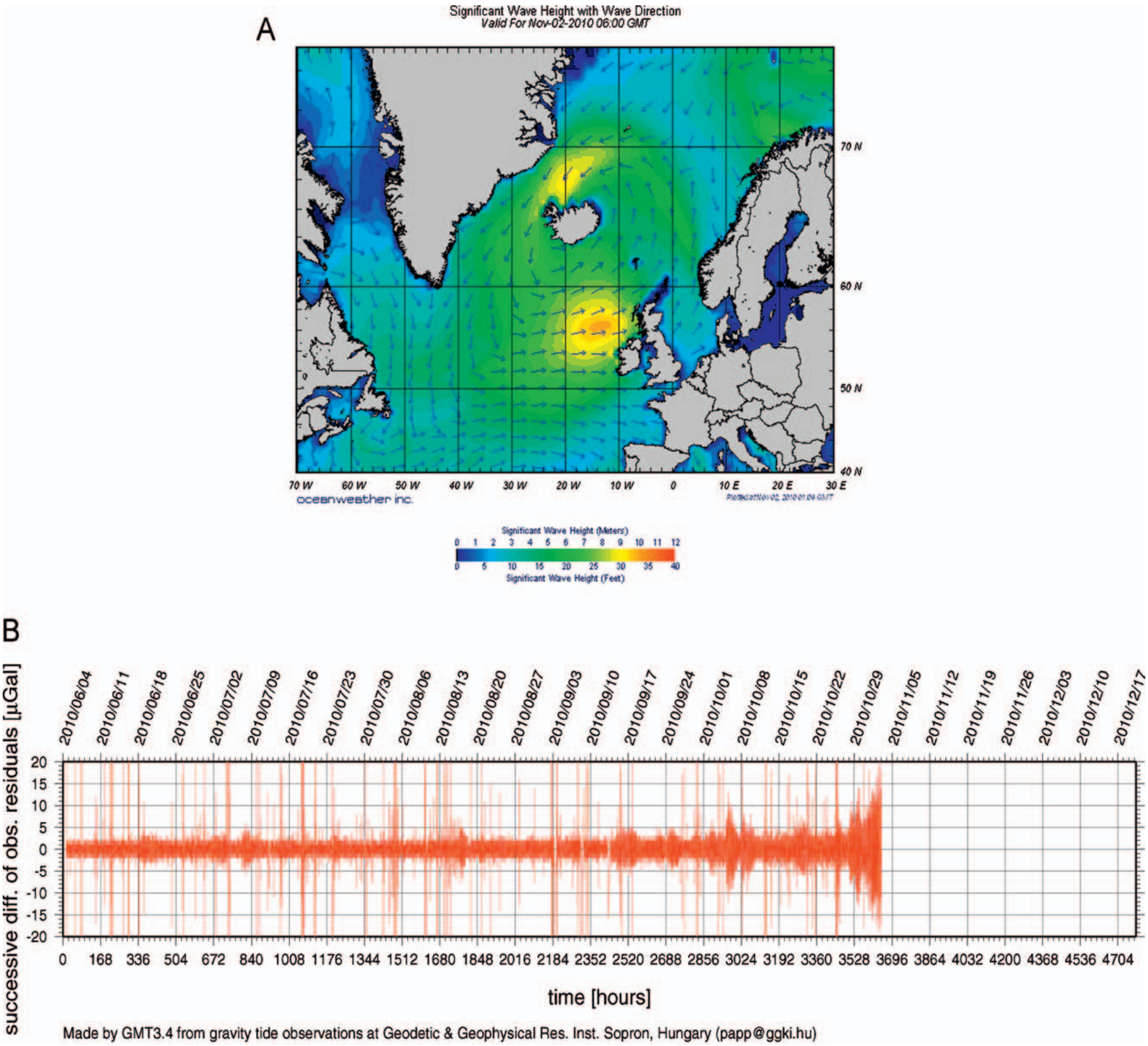

Fig. 8. Ocean weather map (top) and the noise of gravity tide observations in Sopronbánfalva Geodynamical Observatory (bottom) on 02.11.2010. The arrows show the wave directions.

These parameters were derived from the maps of H_{sw} distributed as GIF format images using digital image processing tools provided by MATLAB (Gonzáles et al., 2004). The colour scale coded wave heights were used to select wave height intervals for the analysis. Segmentation of the images according to the predefined intervals was accomplished by a method based on pixel connectivity utilizing 4-connected neighbourhood type. After segmentation of images into regions with given wave heights several statistical parameters can be determined for them. Special attention was paid to compute the area and centre of each storm region since the wave maps are given in Mercator projection which distorts horizontal size of objects depending on latitude with increasing scale from the Equator. The area represented by the maps is bounded by meridians 70W and 30E and parallels 40N and 75N and the content of the maps is discretized on a matrix of 431 pixels × 594 pixels. Therefore the area of a single pixel varies between 98.8 km^2 and 11.3 km^2 for the minimum and maximum latitudes corresponding to the extension of the investigated area, respectively. The coordinates of the barycentre of the waving water mass can be transformed from the image coordinate system to geographical coordinates and distance and azimuth between these points and Sopronbánfalva Geodynamical Observatory ($\lambda = 16.6^\circ$, $\varphi = 47.6^\circ$) were determined as Fig. 9 illustrates it. Inspecting the maximum wave height values for each day (Fig. 10) it is clearly visible that there is a definite difference between summer and autumn–winter periods when the maximum significant wave height could reach more than 10 m for the latter case. It is in a good accordance with the results based on the investigation of body waves (P waves) of microseismic origin on a global scale in a one year long time period (Gerstoft et al., 2008). Similar seasonal variation of the gravity observation noise can be seen also in Fig. 3.

After the determination of the geographical coordinates of storm centres, their distance D to the observation place Sopron, swelling water mass around the storm centres, observation azimuth of the storm centres (Fig. 9) the daily observation noise levels were correlated to these parameters in different combinations.

At first glance Fig. 11 shows a weak control of the water mass (which is now simply represented by its volume, and called significant wave volume later on) disturbed by storm against the distance.

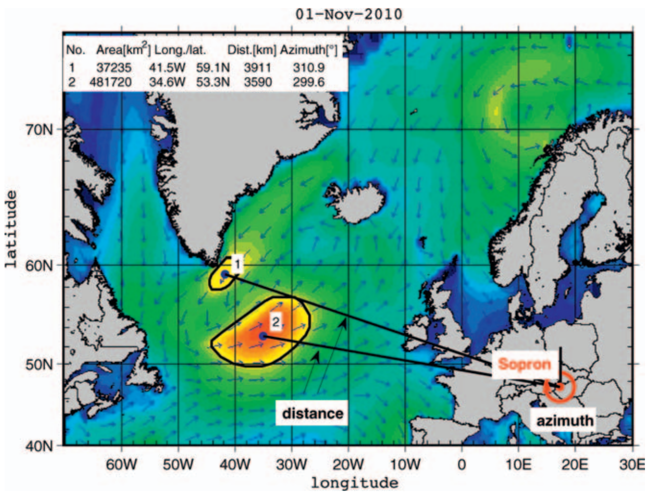

Fig. 9. Geometrical parameters of the spatial relation between observation point and storm regions on 01.11.2010. The areas encircled by black line show subregions, where $H_{sw} \geq 9.5$ m.

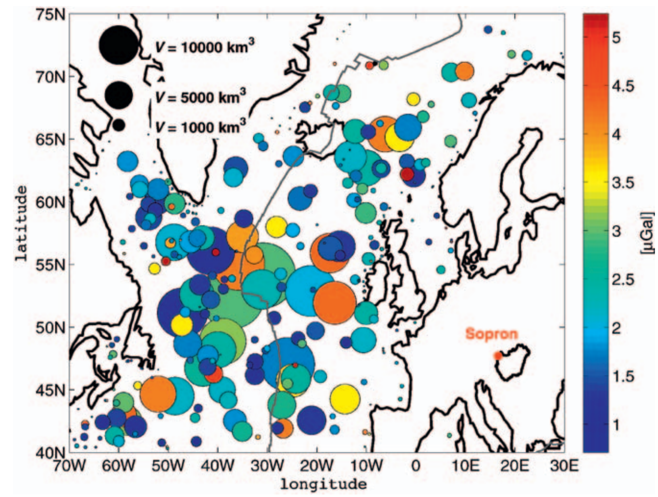

Fig. 12. Geographical distribution of storm centres marked by coloured circles. The colour and the diameter of the circles represent the gravity noise level and the significant wave volume, respectively. The grey line shows the North Atlantic Ridge. Coordinates are in arc degrees.

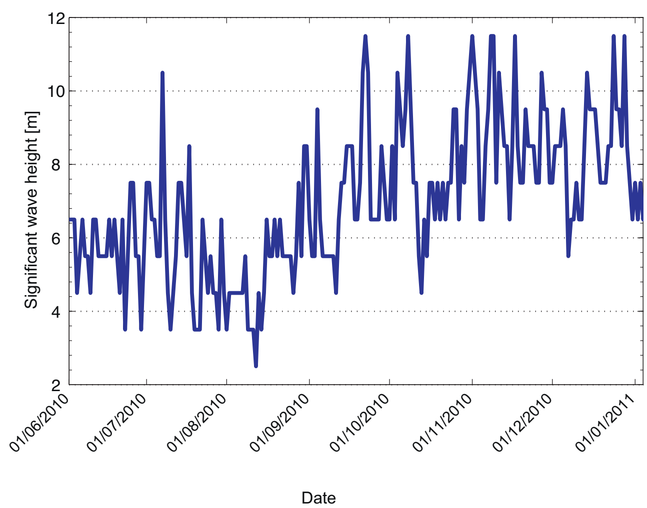

Fig. 10. The seasonal distribution of the daily maximum significant wave heights in the time period of investigation for the area defined in Fig. 9.

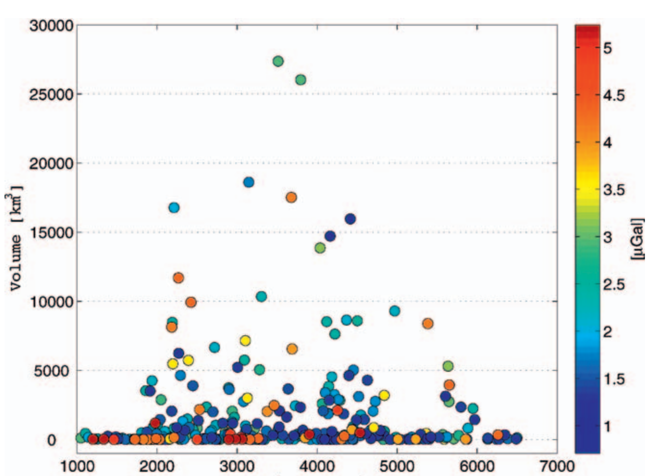

Fig. 11. The distance- and significant wave volume dependence of gravity noise level.

The significant wave volume V_{sw} of a specific storm zone was calculated as the product of the area affected by storm with H_{sw}:

$$V_{sw} = \sum_{i=1}^{M} S_i (H_{sw})_i \tag{18}$$

where $H_{sw} \geq 6.5$ m, S_i and $(H_{sw})_i$ are the area and the significant wave height belonging to the image pixel with index i, respectively. The M pixels forming the specific storm area were identified by segmentation of the images based on the above mentioned pixel connectivity algorithm (see the encircled sub-regions in Fig. 9).

The control of distance is expected somehow in a "the closer the storm the larger its influence" manner but this assumption is not sufficiently justified. This, however, is not a surprise knowing that in some situations the intensity of wave–wave interactions are amplified by the bathymetry according to the "organ pipe resonance" (Kedar et al., 2008; Hillers et al., 2012). For some reasons the occurrence of triggering events generating high gravity observation noise seems to be concentrated at certain distances regardless the size of significant wave volume involved. Although the number of events during the 214 days of observations investigated is enough only for getting preliminary ideas, the characteristic distances, where both large and small storms generated high noise ($\sigma > \pm 3.5$ μGal) can be identified. The shortest distance (1300 km) agrees well with the average distance between the North Atlantic coastline of Western Europe and Sopron. There are further significant source concentrations at distance of 1800–2200 km, 3000 km and 4500 km.

Even if the significant wave volume has no primary influence on the gravity noise level, the distance alone cannot be the basic descriptive parameter in the relation being investigated. Therefore a location map of triggering events was created in order to analyse the connection among the geographical distribution of storm centres, the significant wave volume and the noise level (Fig. 12). It shows a concentration of the geographical locations of events generating high gravity noise, which partly explains both the virtual concentration according to distance (Fig. 11) and the secondary importance of the significant wave volume. Some of the events having considerable effect may somehow be related to tectonic structures (a segment of the North Atlantic Ridge for example). The closest and most disturbing events have very small significant wave volume; consequently these cannot be identified easily in

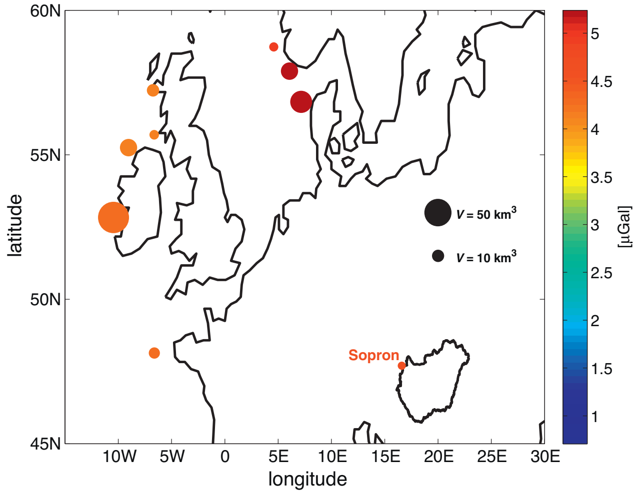

Fig. 13. Identified coastal storm centres generating high gravity noise level ($\sigma > \pm 3.5\,\mu$Gal) at Sopron, Hungary during the time period investigated. The diameter of the circles is proportional to the size of significant wave volume (see the in-map legend). Coordinates are in arc degrees.

Fig. 12. Therefore a part of the Western European coastal area is enlarged in Fig. 13. It supports the general separation of the sources into the class of coastal wave loading and the class of standing waves being formed on the oceans' open surface (Longuet-Higgins, 1950).

Three other possible centres ($\sigma > \pm 3.5\,\mu$Gal) can be seen in Fig. 12. One is located between Iceland and the Norwegian coast where there is a depression of the ocean bottom. The second is about in half way between the British Isles and the North Atlantic Ridge. The third is situated close to the north-eastern coastline of North America where the continental shelf starts approximately. These dominant triggering event locations do not contradict the so called bathymetry-dependent amplification factor maps of wave–wave interaction intensities (Longuet-Higgins, 1950) determined by Hillers et al. (2012) from a global scale comparison of seismic observations and wave action models (Hillers et al., 2012, Fig. 1).

6. Conclusions

The noise in the time series of gravity tides recorded with an experimental installation of the LCR G949 gravity meter equipped with a CCD ocular in the period between 08.06.2010 and 04.01.2011 showed strong correlation with the variable background noise level (microseisms) indicated by a seismograph operated also in Sopronbánfalva Geodynamical Observatory. The RMS gravity noise level is about $\pm 1\,\mu$Gal on "silent" days when the noise is generated mainly by high frequency tremors ($f > 1$ Hz) of the Earth surface. The amplitude spectra of seismograms show that the amplitudes of these oscillations are rarely reach 0.1 nm level. The increased gravity noise, however, is characterized by $\pm(4–5)\,\mu$Gal RMS value when the periodical deformations of the ground have amplitudes greater than 10 nm in the frequency range between 0.05 Hz and 2.5 Hz, as it is indicated also by the spectral analysis of seismograms. It is typically generated by the weather related processes of the hydrosphere in the North Atlantic and North Sea regions. Although the correlation of ocean weather and microseisms has been known for a long time in seismology, its quantitative effect on gravity observations has been underestimated and neglected in the Carpathian–Pannonian basin because of the large distance ($D > 1000$ km) between the possible locations of triggering events and the observation places. The joint analysis of ocean weather maps and gravity data clearly showed that the impact of both the near coast waves hitting directly the coastline of the North Sea ($D < 1500$ km) and the distant events ($D > 3000$ km) of the northern hydrosphere can disturb the gravity observations producing equal gravity noise level in Sopron. Although only records of half a year were analysed and the approach used is phenomenological the geographical distribution of the locations related to dominant noise sources shows a kind of systematic pattern. It fits to the results of more sophisticated global analysis of microseisms based on wave action models, wave–wave interaction models and seismological observations from worldwide arrays.

The comparative analysis of gravity and seismic records through the application of an elementary single wave deformation model also demonstrated that high precision gravimetry ($\sigma \leq \pm 5\,\mu$Gal) is significantly influenced by ocean waves and winds even in the middle of the European continent where it was not really expected. Obviously, the unfavourable effect of microseisms can be efficiently decreased or compensated by proper observation techniques and instrumentation which should be adjusted to the nature of the observed noise. The permanent monitoring and analysis of microseisms in gravimetry may help to understand its characteristics in the Carpathian–Pannonian basin so it is the first step to manage the problem of noise reduction in gravity observations.

Acknowledgements

The authors gratefully thank the supports of TÁMOP 4.2.1/B-09/1/KONV-2010-0006 Project of the University of West Hungary and the National Scientific Research Fund OTKA K 101603. The great help of Zoltán Gráczer, researcher of "Kövesligethy Radó" Seismological Observatory, MTA CSFK GGI who pre-processed the analysed seismological records is also appreciated. The kind comments of Gregor Hillers, Institut des Sciences de la Terre, Université Joseph Fourier on our manuscript helped the authors a lot to broaden their knowledge about the driving mechanism of microseisms. The remarks and suggestions from an anonymous reviewer are greatly appreciated as well. The magnificent contribution of Oceanweather Inc. whose web-distributed maps were extensively used in this research is thankfully acknowledged, too. The proper operation of the monitoring system was guaranteed by Frigyes Bánfi, electrical engineer of MTA CSFK GGI.

References

Baker, T.F., 1984. Tidal deformations of the Earth. Science Progress 69, 197–233.

Gerstoft, P., Shearer, P.M., Harmon, N., Zhang, J., 2008. Global P, PP and PKP wave microseisms observed from distant sources. Geophysical Research Letters 35, L23306, http://dx.doi.org/10.1029/2008GL036111.

Gonzáles, R.C., Woods, R.E., Eddins, S.L., 2004. Digital Image Processing Using MATLAB. Pearson Prentice Hall, p. 609.

Hillers, G., Graham, N., Campillo, M., Kedar, S., Landés, M., Shapiro, N., 2012. Global oceanic microseism sources as seen by seismic arrays and predicted by wave action models. Geochemistry, Geophysics, Geosystems 13 (1), Q01021, http://dx.doi.org/10.1029/2011GC00387.

Kedar, S., Longuet-Higgins, M., Webb, F., Graham, N., Clayton, R., Jones, C., 2008. The origin of deep oceanic microseisms in the North Atlantic Ocean. Proceedings of the Royal Society 464, 777–793.

Kedar, S., 2011. Source distribution of ocean microseisms and implications for time dependent noise tomography. Comptes Rendus Geoscience 343, 548–557.

Longuet-Higgins, M.S., 1950. A theory of the origin of microseisms. Philosophical Transactions of the Royal Society of London A 243, 1–35.

Melchior, P., 1966. The Earth Tides. Pergamon Press, Oxford, p. 458.

Mentes, Gy., Eper-Pápai, I., 2006. Investigation of meteorological effects on strain measurements at two stations in Hungary. Journal of Geodynamics 41 (1–3), 259–267.

Meskó, A., 1984. Digital Filtering: Applications in Geophysical Exploration for Oil. Akadémiai Kiadó, Budapest, p. 636.

Meurers, B., 1987. Comparison of Earth Tide Observations in Vienna. Bulletin d'Informations Mareés Terre 100, 6942–6953.

Meurers, B., van Camp, M., Petermans, T., 2007. Correcting superconducting gravity time-series using rainfall modelling at the Vienna and Membach stations and application to Earth tide analysis. Journal of Geodesy 81 (11), 703–712.

Papp, G., Battha, L., Bánfi, F., 2009. CCD ocular system for LaCoste–Romberg G meters. Geomatikai Közlemények 12, 83–90 (in Hungarian with English abstract).
Pálinkáš, V., 2006. Precise Tidal Measurements by Spring Gravimeters at the Station Pecný. Journal of Geodynamics 41 (1–3), 14–22.
Press, W.H., Flannery, B.P., Teukolsky, S.A., Vetterling, W.T., 1986. Numerical Recipes. The Art of Scientific Computing. Cambridge University Press, London, p. 818.
Torge, W., 2001. Geodesy. Walter de Gruyter, Berlin/New York, p. 416.
Tóth, L., Mónus, P., Zsíros, T., Bus, Z., Kiszely, M., Czifra, T., 2010. Hungarian Earthquake Bulletin. GeoRisk-MTA GGKI, Budapest, p. 140.
Varga, P., Pícha, J., Šimon, Z., 1977. Investigation of gravimetric records at non-tidal frequencies. Studia Geophysica et Geodaetica 21 (2), 195–200.
Varga, P., Gerstenecker, C., Groten, E., Hönig, W., 1985. Gravimetric Earth tide observations in Tihany, reliability and interpretation. Annales Geophysicae 4 (3), 493–498.
Wenzel, H.G., 1996. The nanogal software: Earth tide data processing package – Eterna3.30. Bulletin D'informations Marees Terrestres 124, 9425–9439.
Woo, S.Y., Choi, I.M., Song, H.W., 2007. Measurement of gravitational acceleration values at the calibration laboratories in Korea. In: Proceedings of the 20th Conference on Measurement of Force, Mass and Torque (together with 3rd Conference on Pressure Measurement & 1st Conference on Vibration Measurement), Merida, Mexico, Available at: http://www.imeko.org/publications/tc3-2007/IMEKO-TC3-2007-112u.pdf.